# Stochastic MPC for Charging Control of Lithium Ion Batteries

Anirudh Kyatham[a], Noah Miller[a], Saroj Paudel [a]

[a]*Department of Automotive Engineering, Clemson University, SC*
*akyatha@g.clemson.edu, nhmille@g.clemson.edu, sarojp@g.clemson.edu*

**Abstract**

Lithium-ion batteries have a wide range of applications, from consumer electronics to automotive applications, grid energy storage etc. Safe and efficient operation of the battery and fast charging without compromising the lifetime are some of the critical issues. In this work, we model a lithium-ion battery using a second-order equivalent circuit model and propose a stochastic model predictive control-based charging approach. The stochastic approach showed an improved result over the nominal one when dealing with disturbances. Fast charging without an active cooling mechanism did not have significant advantages over normal charging operation as it was constrained by the maximum allowed core temperature. The battery degradation, on the other hand, almost doubled for fast charging. A compromised charging rate of 2C seemed to be more appropriate. In addition, a simulation result of degradation over 1000 charging cycles at this rate was approximately 12%.

**Keywords: stochastic MPC, constraint-tightening, battery degradation, ECM battery model, fast charging**

## 1. Introduction

Accurate modeling of a lithium-ion battery is difficult due to complex battery dynamics and unmeasurable internal states. Battery dynamics primarily include electrical, electrochemical, thermal and aging processes. Various model-based approaches of varying complexity have been proposed with considerable success in terms of simulation, optimization, estimation and control [1]. Model-based approaches can be broadly classified into equivalent circuit models (ECMs) [2; 3; 4; 5] and physics-based models[6; 7; 8].

ECMs ignore the underlying electrochemical and ion-diffusion process that occurs inside the battery while charging and discharging and fit the electrical behavior by assuming an ideal voltage source and several resistors and capacitors, resulting in a relatively simpler model that is easier to parameterize. The existing studies widely use first (1RC) and second-order (2RC) ECMs. A comparison between the 1RC model and 2RC models shows that the latter is better at replicating the dynamic behavior [9]. In these models, lumped electrical parameters are often a function of the state of charge and the temperature of the battery. Numerous charging and discharging tests at different temperatures are used to identify these parameters [10]. Thermal dynamics is usually modeled as a lumped model with thermal resistance and capacitance between the battery core and the enclosure (conduction) and between the battery enclosure and air (convection) [3; 10; 11] while [4] only considers the convective heat transfer without distinguishing the core and the surface. In [9], a relatively complex approach is considered where the heat transfer is modeled as irreversible heat (joule heating), reversible heat (due to phase change) and convective heat transfer to the external. In [3], [10] and [11], coupled electro-thermal models are discussed where a 2RC ECM with three-states and a thermal model with two states are coupled to define a five-state battery model in [4], an ECM with four-states and a thermal model with a single state is used to model the battery dynamics.

Conversely, physics-based models (aka electro-chemical models) use nonlinear coupled partial differential equations (PDEs) derived from the principles of electro-chemistry. The PDEs are temperature dependent, and thus, a separate thermal model is not required as in ECMs. These models are more accurate than the ECMs but also are complex and computationally intensive. Thus, the majority of existing studies primarily use reduced-order models such as the single particle model (SPM). Parameters such as the terminal voltage, $V_T$, battery surface temperature, $T_s$ and the battery current, $I$, can be measured by an external device. However, internal states like the state of charge ($SOC$), open circuit voltage ($V_{ocv}$), state of health ($SOH$) and battery core temperature, $T_c$, are not measurable and need to be estimated. In addition, these parameters are stochastic. Existing studies [11; 6; 7; 3; 4] mainly use extended Kalman Filter (EKF) while [8] uses Unscented Kalman Filter (UKF).

In this paper, we formulate the Li-ion battery charging problem as a stochastic MPC problem. In addition, we explore the SoH estimation using empirical methods and compare it for different charging rates. Section 2 describes the 2RC ECM model of Li-ion battery, followed by the description of EKF-based state estimation in section 3. In section 4, we first define the stochastic MPC problem and derive the deterministic counterpart for computation. This is followed by the simulation results for six different cases, *viz*. nominal MPC without disturbances, nominal MPC with disturbances and stochastic MPC with disturbance for two different charging rates, 1C and 5C.

## 2. Battery Modeling

### *2.1. Equivalent Circuit Model*

An ECM was chosen to model the electrical dynamics of the battery over a physics-based model due to its tractable nature and comparative ease of modeling. A 2RC model was chosen over a 1RC due to an improvement in accuracy to real data as this model can account for both slower and faster dynamics [9]. A 2RC ECM is shown in Fig. 1 where the parameters $R_0$, $R_1$, $C_1$, $R_2$ and $C_2$ are functions of the $SOC$ and temperature and usually identified experimentally. In this paper, we refer to the results presented in [11] for these temperature and SOC-dependent parameters.

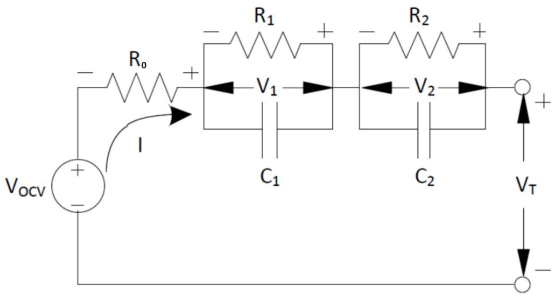


Figure 1: Equivalent Circuit Model ([9])

The differential equation for the $SOC$ and voltage across the two capacitors are shown in equations (1), (2) and (3), respectively, where $Q_{batt}$ is the Ampere hour capacity of the battery, I is the current and $V_1$ and $V_2$ are the voltage across the capacitors. The current I is assumed to be negative for charging. Using Kirchoffs' law, we can write the relationship between $V_{ocv}$ and the battery terminal voltage $V_T$ as in (4). In [7], $V_{ocv}$ is approximated by a sixth-order polynomial function of SOC, $f_6$.

$$\dot{SOC} = \frac{-1}{Q_{batt}} \cdot I \tag{1}$$

$$\dot{V}_1 = -\frac{1}{R_1 C_1} \cdot V_1 + \frac{1}{C_1} \cdot I \tag{2}$$

$$\dot{V}_2 = -\frac{1}{R_2 C_2} \cdot V_2 + \frac{1}{C_2} \cdot I \tag{3}$$

$$V_T = V_{ocv} - V_1 - V_2 - I \cdot R_s \tag{4}$$

$$V_{OCV} = f_6(SOC) \tag{5}$$

### 2.2. Thermal Model

The Thermal model of a cylindrical cell is shown in Fig. 2 as a lumped model and represented by equation (6-8). $Q_{gen}$ is the joule heat generated inside the cell during charging while $T_c$, $T_s$ and $T_{air}$ are, respectively the core, surface and air temperature. $R_c$ and $R_s$ are the core and surface conduction resistances, $C_c$ and $C_s$ are the core and surface thermal capacitance. An average of $T_c$ and $T_s$, $T_m$ is used to estimate the parameters of the electrical model.

$$Q_{gen} = I(V_{ocv} - V_T) \tag{6}$$

$$\dot{T}_c = \frac{Q_{gen}}{C_c} + \frac{T_s - T_c}{C_c R_c} \tag{7}$$

$$\dot{T}_s = \frac{T_{air} - T_s}{C_s R_s} - \frac{T_s - T_c}{C_s R_c} \tag{8}$$

### 2.3. Coupled Model

The two models are coupled together to facilitate connections between the electrical and thermal dynamics. The thermal model takes $Q_{gen}$ and $T_{air}$ as inputs and provides $T_m$ to the electrical model so the electrical parameters can be updated as depicted in Fig. 3.

$$\dot{x} = f(x,u) = \begin{bmatrix} \dot{SOC} \\ \dot{V}_1 \\ \dot{V}_2 \\ \dot{T}_c \\ \dot{T}_s \end{bmatrix} = \begin{bmatrix} -\frac{1}{Q_{\text{batt}}} I \\ -\frac{1}{R_1 C_1} V_1 + \frac{1}{C_1} I \\ -\frac{1}{R_2 C_2} V_2 + \frac{1}{C_2} I \\ \frac{V_1 I + V_2 I + R_0 . I^2}{C_c} + (T_s - T_c)\left(\frac{1}{R_c C_c}\right) \\ \frac{T_{\text{air}} - T_s}{C_s R_s} - \frac{T_s - T_c}{C_s R_c} \end{bmatrix}$$

$$y = h(x,u) = \begin{bmatrix} V_t \\ T_s \end{bmatrix} = \begin{bmatrix} V_{ocv} - V_1 - V_2 - IR_0 \\ T_s \end{bmatrix}$$

where, $x = [SOC \quad V_1 \quad V_2 \quad T_c \quad T_s]'$ is the state vector and $u = I$ is the control input.

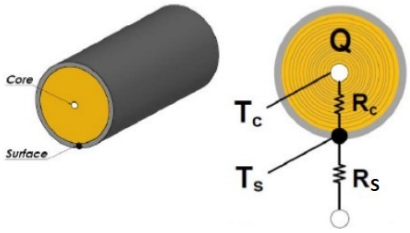


Figure 2: Thermal Model ([9])

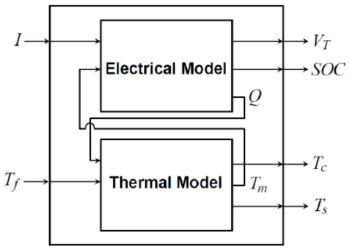


Figure 3: Coupled Model([9])

### 2.4. Uncertainties and Disturbances

The model formulated in the preceding subsection does not involve any uncertainties in modeling and disturbances. However, in real battery charging scenario, there are always some uncertainties and disturbances, e.g. uncertainties in the model parameters, disturbance in the input current, variation in the ambient temperature etc. In addition to this, there are measurement errors due to the limitations of the sensors. The first two disturbances are modeled together as an additive disturbance $w_t$, (aka process noise), and the measurement errors are modeled as additive measurement noise, $v_t$. Both $w_t$ and $v_t$ are assumed white noise and follow Gaussian distribution with variance $Q_w$ and $R_v$ respectively. The variation in ambient temperature is a slow process and thus is modeled as a sinusoid about a reference ambient temperature.

$$\dot{x}(t) = f(x,u) + w_t \tag{11}$$

$$y(t) = h(x,u) + v_t \tag{12}$$

$$T_{amb} = T_{amb,ref} + A_d \sin(\omega t) \tag{13}$$

## 3. State Estimation

Some of the states, like the temperature at the core of the battery and the SoC cannot be measured directly and thus need to be estimated. Since the system dynamics are nonlinear, EKF is chosen over the traditional KF to estimate these states. The EKF linearizes the system dynamics and the measurement model locally and applies the KF to estimate the states. KF

involves two steps: the prediction step where the next state is predicted based on the system dynamics and current state and control inputs and the correction step which is performed once the measurement is available. In the following, the EKF formulation for the discretized system of the continuous model shown in equations (9) and (10) is shown.

Prediction:

$$\hat{x}_{k|k-1} = f(\hat{x}_{k-1|k-1}, u_{k-1|k-1}) \tag{14}$$

$$\hat{P}_{k|k-1} = F_k P_{k-1|k-1} F_k^T + Q_{k-1} \tag{15}$$

Kalman Gain:

$$K_k = P_{k-1|k-1} H_k^T \left( H_k P_{k|k-1} H_k^T + R_k \right)^{-1} \tag{16}$$

Correction:

$$\hat{x}_{k|k} = \hat{x}_{k|k-1} + K_k \left( y_k - h\left( \hat{x}_{k|k-1}, u_{k-1} \right) \right) \tag{17}$$

$$P_{k|k} = \left( I - K_k H_k \right) P_{k|k-1} \tag{18}$$

where $F_k$ and $H_k$ are the Jacobian matrices of the system dynamics and the measurement model evaluated at the current state, that linearize the system in its proximity and given by equation (19) and $y_k$ is the measurement at time step $k$.

$$F_k = \left. \frac{\partial f}{\partial x} \right|_{\hat{x}_{k-1|k-1}, u_{k-1}}, H_k = \left. \frac{\partial h}{\partial x} \right|_{\hat{x}_{k|k-1}} \tag{19}$$

The above formulation of state estimation does not include the SoH estimation because SoH has slower dynamics and requires hundreds of charge-discharge cycles to get meaningful insight. It is assumed that SoH is constant throughout one charging. However, for an accurate estimation of the useful capacity and performance of the battery over time, SoH estimation is important. A semi-empirical model that uses Arrhenius equation and is presented in [12] is considered. The model evaluates the capacity fade as a function of ampere-hour throughput (Ah) over the lifetime of the battery and is given by equation (20).

$$f_c(SOC, T_m) = A_c(SOC, T_m) \cdot \exp\left( -\frac{E_{ac}}{R_g \cdot T_m} \right) \tag{20}$$

$f_c(SOC, T_m)$ is a nonlinear function for the ageing factor expressed as a function of SoC and temperature. Parameter $A_c$ is the capacity severity factor of the battery, $E_{ac}$ is the cell activation energy, $R_g$ is the universal gas constant and $T_m$ is the average temperature of the cell. $E_{ac}$ and $A_c$ are obtained from fitting of experimental results.

The accumulated capacity loss, $S_{loss}$ and the current capacity, $S$ are then calculated as:

$$S_{loss}(Ah) = f_c(SOC, T_m) \cdot Ah^z \tag{21}$$

$$S(Ah) = S_{in} \left( 1 - \frac{S_{loss}(Ah)}{100} \right) \tag{22}$$

where $S_{in}$ is the initial SoH and, without the loss of generality, will be assumed one and $z$ is determined experimentally.

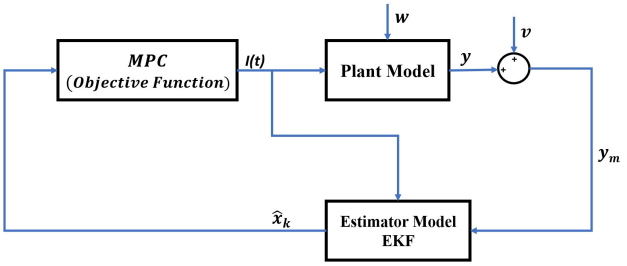


Figure 4: MPC Model for Charging Control

## 4. MPC formulation for charging control

The block diagram for the MPC-based charging control is shown in Figure 4. The plant model represents the coupled electro-thermal model. An EKF-based estimator is used to estimate the states that are not measurable. Since the process and measurement noise are random variables (assumed zero-mean Gaussian with variance of $\Sigma_w$ and $\Sigma_v$, respectively), the state trajectories and control input are also random variables. As a result, the performance of the controller will be assessed based on the expected value of the objective function over the time horizon. Considering a fast charging application, a *pseudo min time* objective function that tries to reach the specified SoC target as fast as possible is adopted.

$$E[J(x, u)] \tag{23}$$

$$J(x, u) = \sum_{k=0}^{N-1} \| SOC_{target} - SOC_k \|_Q \tag{24}$$

Unfortunately, due to stochasticity, the system constraints cannot be considered deterministically; the stochasticity may result in a non-zero chance of violating the constraints. Consequently, the constraints need to be considered in a probabilistic sense. A measure of the risk of constraint violation is introduced, and the constraints are now required to be satisfied to a certain probability limit.

$$\Pr\left( G(x, u) \leq g \right) \geq 1 - \varepsilon \tag{25}$$

where $G(x, u) \leq g$ is the polyhedra for the original constraints. The stochastic problem can then be written as:

$$\min_{x,u} \quad E[J(x, u)] \tag{26}$$

Subject to:

$$x^+ = f(x, u) \tag{27}$$

$$\Pr\left( G(x, u) \leq g \right) \geq 1 - \varepsilon \tag{28}$$

The violation probability, $\varepsilon$, may differ for each constraint. However, for the sake of simplicity, we assume it to be uniform for all constraints. The stochastic problem in (26) cannot be solved directly. We thus rely on the chance constraint (CC) method to tighten the original constraints such that the original constraints are probabilistically satisfied with a violation probability, $\varepsilon$, despite external disturbances such as variation in ambient temperature etc. For this problem, we assume $\varepsilon = 0.05$. The selected probability threshold, $\varepsilon$, was chosen to

maintain a high likelihood of constrained satisfaction but allow for balanced performance. The deterministic set of constraints for which the original set of constraints are stochastically satisfied for the given $\varepsilon$ is given by:

$$[G]_j x_k \leq [g]_j - \gamma_j \tag{29}$$

$$\gamma_j = \sqrt{[G]_j \Sigma_k [G]_j'} F^{-1}(\varepsilon), \quad j = 1, 2...J \tag{30}$$

where, $\gamma_j$ is called the back off parameter for the $j^{th}$ constraint. Since the process noise and the measurement noise are assumed Gaussian, $F^{-1}(\varepsilon)$ is the quantile function and given by the inverse CDF of normal distribution [13].

Applying the tightened chance constraints to the original objective function allows a deterministic solution to the original stochastic problem. The solution will guarantee original constraint satisfaction of 95% for each time step in the horizon. The deterministic MPC is written as:

$$\min_{x_k, u_k} \sum_{k=0}^{N-1} \|SOC_{target} - SOC(k)\|_Q \tag{31}$$

Subject to:

constraint (27)

$$u_k \in \bar{\mathbb{U}} \subseteq \mathbb{R}, \quad k = 0, 1...N-1 \tag{32}$$

$$_k \in \bar{\mathbb{X}} \subseteq \mathbb{R}^5, \quad k = 1, 2, ...N \tag{33}$$

where the constraints (32) and (33) represent the tightened constraints in a compact form.

## 5. Simulation and Results

### 5.1. Constraint Selection

Constraints to encourage a high SOH for the battery and enforce safe operating conditions were implemented in the MPC framework. The upper SOC threshold was constrained to 90% , a common compromise between capacity utilization and mitigating lithium deposition, one of the main sources of accelerated LIB ageing [14; 15; 16]. For Depth of Discharge (DoD) $< 80\%$, calendar ageing dominates cyclic ageing, isolating the constraints to prioritize. This provided guidance for setting the lower SOC bound at 15% since calendar ageing is more desirable.

Core temperature management is integral to maintaining battery health with extreme circumstances being dangerous due to thermal runaway [15]. A modest increase in the ageing rate up to 65°C, beyond that will accelerate ageing rapidly[17]. The surface temperature is also constrained with a slightly smaller value [15]. As a result, the upper bounds on the core temperature, $T_c$ and surface temperature, $T_s$ are set to 65°C and 40°C, respectively. These constraints will ensure the battery maintains within a safer operating envelope.

It is often assumed that lower average temperatures favor longevity, yet empirical evidence shows inconsistent ageing for temperatures below 25°C—some studies report accelerated ageing, while others suggest it is where ageing is optimal [17]. This discrepancy highlights the complex interplay between ageing mechanisms, which can vary with temperature. At lower temperatures, the predominant issue is lithium plating, while at higher temperatures, the degradation of the cathode and the solid-electrolyte interphase (SEI) becomes more prominent [18; 19]. This provides a lower bound for $T_s$ and $T_c$ to be 20°C.

The applied charging current was also constrained based on the charging mode. Charging modes are specified by the C-rate, which scales the applied current to the battery size. Slow-charging is specified at 1C, targeting an hour-long charge time [15].

### 5.2. Result and Discussion

Figure 5 presents the results for applying nominal MPC to battery charging with no disturbance considered. In both fast and slow-charging modes, we observe an expected constant rate. The main deviation from this is that fast-charging (5C) attempts a higher rate before being restricted by temperature constraints, leading to a reduced rate for the remainder of the cycle, whereas slow-charging (1C) is able to maintain a constant rate for the whole cycle. The inactivity of temperature constraints at 1C is seen for the entire cycle (Figure 5a). This is in contrast with Figure 5b, showing active temperature constraints for nearly the entire cycle at 5C. This regulation impedes charging performance, leading to a prolonged charging cycle.

With the introduction of disturbances, the temperatures show only minor fluctuations throughout (Figure 6). The EKF is observed to overestimate the temperature slightly. Despite the disturbances, Figure 6a shows charging at 1C satisfies constraints. For fast-charging, the addition of disturbance coupled with persistently active constraints poses a heightened risk of constraint violation. This suggests the MPC may require additional careful tuning to ensure the battery remains within allowable limits.

Examining Figure 7, stochastic MPC mirrors the actions of nominal MPC. Temperature constraints remain inactive for 1C charging, indicating no active cooling would be needed. Conversely, 5C charging shows temperature constraints being active (Figure 7b), mirroring the nominal setup results. This limitation hints at the necessity of active cooling to enhance charging performance and ensure a high SOH under these more demanding conditions. Addition of stochastic chance constraints does not seem to improve performance compared to nominal MPC. In fast-charging, the proximity to the upper boundary suggests minimal room for meaningful improvement. If the system thermal response was disturbed upwards, constraint violation is a distinct possibility. Due to SOH degradation often considered minimal at 25°C, slow-charging may be the best charging protocol for prioritizing SOH. Fast-charging does indeed complete the cycle faster but carries significant risk as a trade-off.

SOH degradation over a single charge cycle for different charging modes is shown in Fig. 8a. Degradation was found to increase for higher charging rates. However, charging rate of 2C showed a better trade-off in terms of charging time and battery degradation. A long-term degradation simulation was also performed, and the battery underwent 1000 cycles at 2C. The results show a gradual degradation to 88% of its original capacity. The findings are reasonably consistent with empirical data, however, it is notable the tapering off was not accounted for. The simulation was computationally expensive so it was

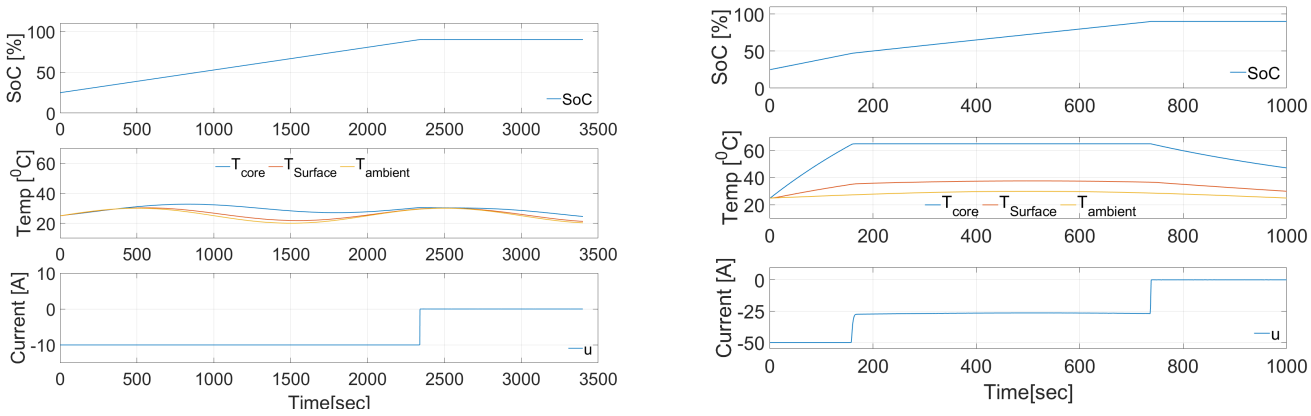


(a) (b)

Figure 5: SOC, temperature and input current for nominal MPC without disturbance (a) Maximum C-rate = 1C (b) Maximum C-rate = 5C

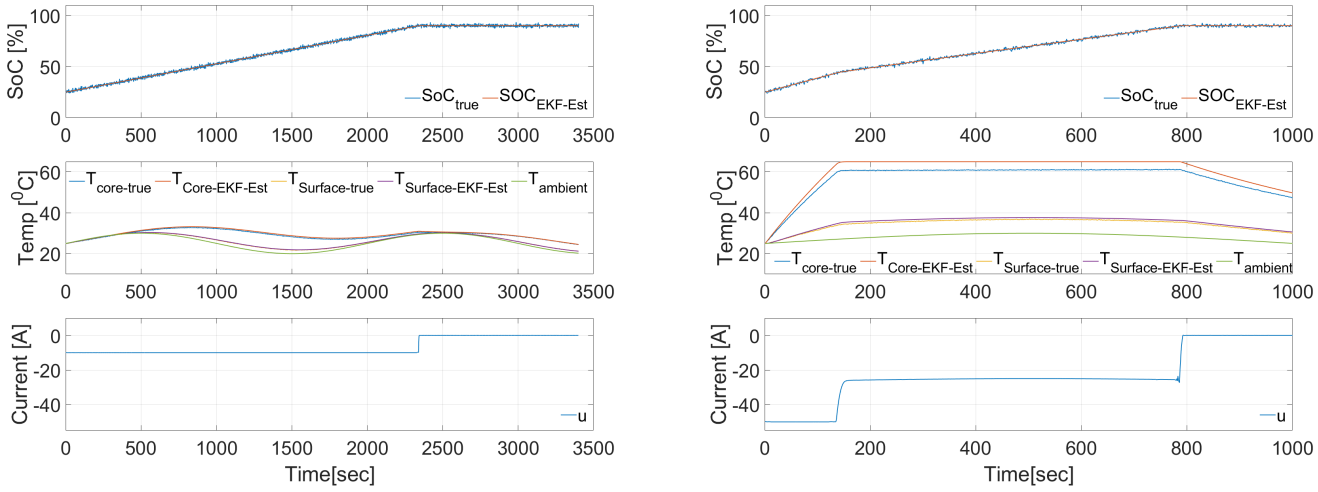


(a) (b)

Figure 6: SOC, temperature and input current for nominal MPC with disturbance (a) Maximum C-rate = 1C (b) Maximum C-rate = 5C

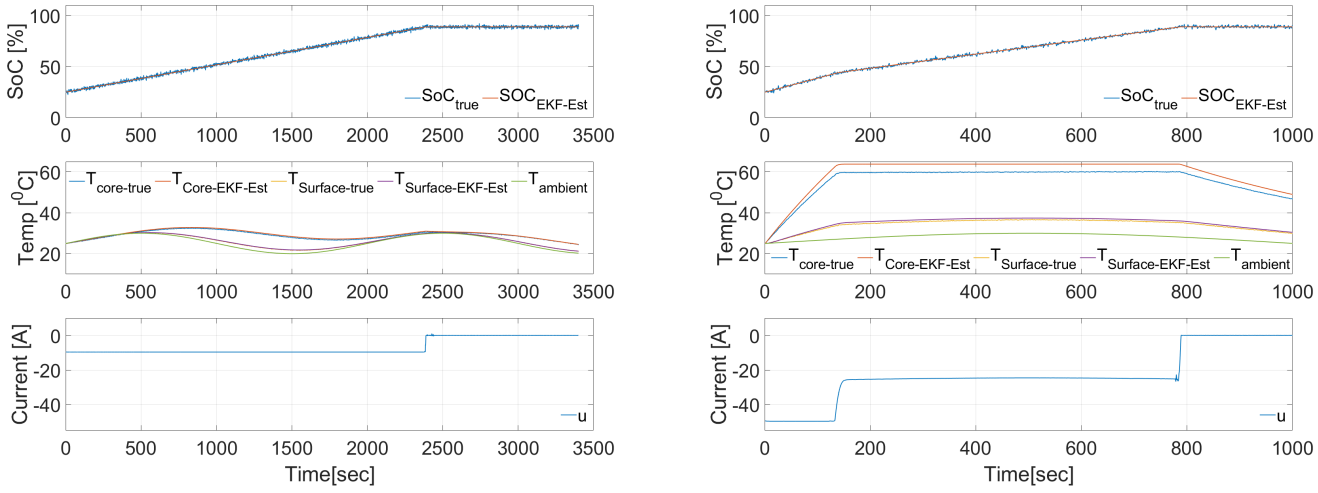


(a) (b)

Figure 7: SOC, temperature and input current for stochastic MPC with disturbance (a) Maximum C-rate = 1C (b) Maximum C-rate = 5C

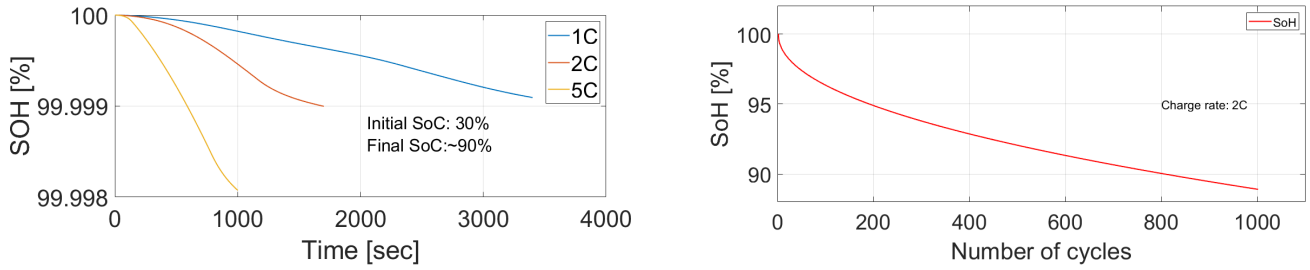


(a) (b)

Figure 8: (a) SoH for different C-rate for one charging cycle (b) SoH after 1000 charging cycles at C-rate=2C

not able to be run for full degradation for varying charge rates. The selected SOH model aligns well with our model's parameters and balances complexity and practical application. Other more accurate SOH estimation models exist; however, they often require detailed cell models involving geometrical and electrochemical parameters [17; 20].

## 6. Conclusion

In this paper, we modeled a Li-ion battery using a second-order equivalent circuit model and proposed a stochastic model predictive control-based charging approach. The stochastic approach showed an improved result over the nominal one when dealing with disturbances and noises. Fast charging without an active cooling mechanism did not have significant advantages over normal charging operation as it was constrained by the maximum allowed core temperature. The battery degradation, on the other hand, almost doubled for fast charging. A compromised charging rate of 2C seemed to be more appropriate. In addition, a simulation result of degradation over 1000 charging cycles at this rate was approximately 12% . The study underscores the importance of a balanced charging strategy, considering factors like temperature constraints and degradation risks, to ensure safe, efficient, and long-term operation of Li-ion batteries.

## References


[1] J. B. Rawlings, D. Q. Mayne, and M. M. Diehl, *Model Predictive Control: Theory, Computation, and Design*. Santa Barbara, California, USA and London, England and Freiburg, Germany: Nob Hill Publishing, 2nd ed., 2017.

[2] M. A. Xavier and M. S. Trimboli, "Lithium-ion battery cell-level control using constrained model predictive control and equivalent circuit models," *Journal of Power Sources*, vol. 285, pp. 374–384, 2015.

[3] H. Bouchareb, K. Saqli, N. K. M'Sirdi, and M. Oudghiri, "Observer design for soc estimation of li-ion batteries based on electro-thermal coupled model," in *2021 9th International Renewable and Sustainable Energy Conference (IRSEC)*, pp. 1–6, 2021.

[4] Y. Lu, X. Han, G. Zhao, L. Lu, and M. Ouyang, "Optimal charging of lithium-ion batteries based on model predictive control considering lithium plating and cell temperature," in *2021 6th International Conference on Power and Renewable Energy (ICPRE)*, pp. 1248–1253, 2021.

[5] N. Tian, H. Fang, and Y. Wang, "Real-time optimal lithium-ion battery charging based on explicit model predictive control," *IEEE Transactions on Industrial Informatics*, vol. 17, no. 2, pp. 1318–1330, 2021.

[6] C. Zou, C. Manzie, and D. Nešić, "Model predictive control for lithium-ion battery optimal charging," *IEEE/ASME Transactions on Mechatronics*, vol. 23, no. 2, pp. 947–957, 2018.

[7] S. Dey, B. Ayalew, and P. Pisu, "Nonlinear robust observers for state-of-charge estimation of lithium-ion cells based on a reduced electrochemical model," *IEEE Transactions on Control Systems Technology*, vol. 23, no. 5, pp. 1935–1942, 2015.

[8] S. Dey and B. Ayalew, "Real-time estimation of lithium-ion concentration in both electrodes of a lithium-ion battery cell utilizing electrochemical–thermal coupling," *ASME Journal of Dynamic Systems, Measurement, and Control*, vol. 139, no. 3, p. 031007, 2017.

[9] R. Stocker, N. Lophitis, and A. Mumtaz, "Development and verification of a distributed electro-thermal li-ion cell model," in *44th Annual Conference of the IEEE Industrial Electronics Society (IECON)*, pp. 2044–2049, 2018.

[10] X. Lin, H. E. Perez, S. Mohan, J. B. Siegel, A. G. Stefanopoulou, Y. Ding, and M. P. Castanier, "A lumped-parameter electro-thermal model for cylindrical batteries," *Journal of Power Sources*, vol. 257, pp. 1–11, 2014.

[11] L. Zhilong and S. Niloofar, "Observer and controller designs for lithium ion batteries," *CE 295 FINAL REPORT*, 2023.

[12] M. Schimpe, M. E. von Kuepach, M. Naumann, H. C. Hesse, K. A. Smith, and A. Jossen, "Comprehensive modeling of temperature-dependent degradation mechanisms in lithium iron phosphate batteries," *Journal of the Electrochemical Society*, vol. 165, 1 2018.

[13] M. Farina, L. Giulioni, L. Magni, and R. Scattolini, "An approach to output-feedback mpc of stochastic linear discrete-time systems," *Automatica*, vol. 55, pp. 140–149, 2015.

[14] R. Hausbrand, G. Cherkashinin, H. Ehrenberg, M. Gröting, K. Albe, C. Hess, and W. Jaegermann, "Fundamental degradation mechanisms of layered oxide li-ion battery cathode materials: Methodology, insights and novel approaches," *Materials Science and Engineering: B*, vol. 192, pp. 3–25, 2015.

[15] A. Romero, A. Goldar, L. D. Couto, J. M. Maestre, and E. Garone, "Fast charge of li-ion batteries using a two-layer distributed mpc with electrochemical and thermal constraints," in *2019 18th European Control Conference (ECC)*, 2019.

[16] H. Zhang, Z. Sun, and W. Gu, "Determination of the soh estimation indicator and the temperature influence on lithium-ion battery in the ev/phev applications," in *2015 IEEE International Conference on Mechatronics and Automation (ICMA)*, (Beijing, China), IEEE, 2015.

[17] S. Yang, C. Zhang, J. Jiang, W. Zhang, L. Zhang, and Y. Wang, "Review on state-of-health of lithium-ion batteries: Characterizations, estimations and applications," *Journal of Cleaner Production*, vol. 314, 2021.

[18] M. Keyser, A. Pesaran, Q. Li, S. Santhanagopalan, K. Smith, E. Wood, S. Ahmed, I. Bloom, E. Dufek, M. Shirk, A. Meintz, C. Kreuzer, C. Michelbacher, A. Burnham, T. Stephens, J. Francfort, B. Carlson, J. Zhang, R. Vijayagopal, K. Hardy, F. Dias, M. Mohanpurkar, D. Scoffield, A. N. Jansen, T. Tanim, and A. Markel, "Enabling fast charging — battery thermal considerations," *Journal of Power Sources*, vol. 367, pp. 228–236, 2017.

[19] T. Waldmann, M. Wilka, M. Kasper, M. Fleischhammer, and M. Wohlfahrt-Mehrens, "Temperature dependent ageing mechanisms in lithium-ion batteries – a post-mortem study," *Journal of Power Sources*, vol. 262, pp. 129–135, 2014.

[20] S. Atalay, M. Sheikh, A. Mariani, Y. Merla, E. Bower, and W. D. Widanage, "Theory of battery ageing in a lithium-ion battery: Capacity fade, nonlinear ageing and lifetime prediction," *Journal of Power Sources*, 2020.

## Appendix

Sixth-degree polynomial equation to approximate the open circuit voltage $V_{ocv}$ in terms of state of charge.

$$\begin{aligned} V_{OCV}(SOC) = {} & 14.7958 \cdot SOC^6 - 36.6148 \cdot SOC^5 \\ & + 29.2355 \cdot SOC^4 - 6.2817 \cdot SOC^3 \\ & - 1.6476 \cdot SOC^2 + 1.2866 \cdot SOC + 3.4049 \end{aligned}$$

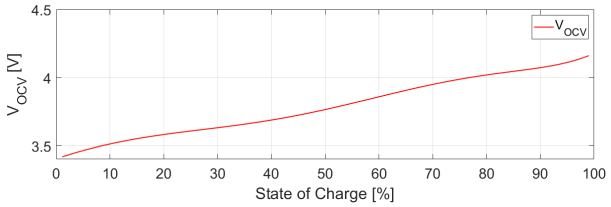


Figure 9: Sixth-order polynomial relationship between $V_{OCV}$ and SOC

Table 1: Simulation Parameters

| **Parameters** | **Value** | **Units** |
|---|---|---|
| $R_{0,\text{nom}}$ | 0.0055 | Ohms |
| $R_1$ | 0.0016 | Ohms |
| $R_2$ | 0.0113 | Ohms |
| $C_1$ | 523.215 | Farad |
| $C_2$ | $6.2449 \times 10^4$ | Farad |
| $Q_{\text{batt}}$ | 10 | Ah |
| $R_c$ | 7.4013 | K/W |
| $C_c$ | 44.07 | J/K |
| $R_s$ | 2.0751 | K/W |
| $C_s$ | 4.5 | J/K |
| $T_{\text{amb,ref}}$ | 298 | Kelvin |
| $A_d$ | 5 | Kelvin |
| $\omega$ | 0.0031 | rad/sec |
| $A_c(\cdot)$ | 557 | - |
| $E_{ac}$ | 22406 | - |
| $R_g$ | 8.314 | J/mol K |
| $z$ | 0.48 | - |
| $S_{\text{in}}$ | 1 | - |
| $u_{\text{min}}$ | 10, 20, 50 | Ampere |
| $u_{\text{max}}$ | 10, 20, 50 | Ampere |
| $\text{SOC}_{\text{min}}$ | 0.15 | - |
| $\text{SOC}_{\text{max}}$ | 0.9 | - |
| $T_{c,\text{min}}$ | 293 (20°C) | Kelvin |
| $T_{c,\text{max}}$ | 338 (65°C) | Kelvin |
| $T_{s,\text{min}}$ | 0 | Kelvin |
| $T_{s,\text{max}}$ | 318 (45°C) | Kelvin |
| $\varepsilon$ | 5% | - |

$$\Sigma_w = \begin{bmatrix} 1 \times 10^{-4} & 0 & 0 & 0 & 0 \\ 0 & 1 \times 10^{-2} & 0 & 0 & 0 \\ 0 & 0 & 1 \times 10^{-2} & 0 & 0 \\ 0 & 0 & 0 & 1 & 0 \\ 0 & 0 & 0 & 0 & 1 \end{bmatrix}$$

$$\Sigma_v = \begin{bmatrix} 4 \times 10^{-2} & 0 \\ 0 & 1 \end{bmatrix}$$